Magn Reson Med Sci 2020; 19; 333–344
doi:10.2463/mrms.mp.2019-0107
Published Online: January 17, 2020

MAJOR PAPER

Assessing the Risk of Intracranial Aneurysm Rupture Using Morphological and Hemodynamic Biomarkers Evaluated from Magnetic Resonance Fluid Dynamics and Computational Fluid Dynamics

Roshani Perera[1], Haruo Isoda[1,2*], Kenta Ishiguro[1,3], Takashi Mizuno[1,4], Yasuo Takehara[5,6], Masaki Terada[7], Chiharu Tanoi[8], Takehiro Naito[8,9], Harumi Sakahara[10,11], Hisaya Hiramatsu[12], Hiroki Namba[12], Takashi Izumi[13], Toshihiko Wakabayashi[13], Takafumi Kosugi[14], Yuki Onishi[15], Marcus Alley[16], Yoshiaki Komori[17], Mitsuru Ikeda[1], and Shinji Naganawa[6]

Purpose: Evaluate *in vivo* hemodynamic and morphological biomarkers of intracranial aneurysms, using magnetic resonance fluid dynamics (MRFD) and MR-based patient specific computational fluid dynamics (CFD) in order to assess the risk of rupture.

Methods: Forty-eight intracranial aneurysms (10 ruptured, 38 unruptured) were scrutinized for six morphological and 10 hemodynamic biomarkers. Morphological biomarkers were calculated based on 3D time-of-flight magnetic resonance angiography (3D TOF MRA) in MRFD analysis. Hemodynamic biomarkers were assessed using both MRFD and CFD analyses. MRFD was performed using 3D TOF MRA and 3D cine phase-contrast magnetic resonance imaging (3D cine PC MRI). CFD was performed utilizing patient specific inflow–outflow boundary conditions derived from 3D cine PC MRI. Univariate analysis was carried out to identify statistically significant biomarkers for aneurysm rupture and receiver operating characteristic (ROC) analysis was performed for the significant biomarkers. Binary logistic regression was performed to identify independent predictive biomarkers.

Results: Morphological biomarker analysis revealed that aneurysm size [$P = 0.021$], volume [$P = 0.035$] and size ratio [$P = 0.039$] were statistically significantly different between the two groups. In hemodynamic biomarker analysis, MRFD results indicated that ruptured aneurysms had higher oscillatory shear index (OSI) [OSI.max, $P = 0.037$] and higher relative residence time (RRT) [RRT.ave, $P = 0.035$] compared with unruptured aneurysms. Correspondingly CFD analysis demonstrated significant differences for both average and maximum OSI [OSI.ave, $P = 0.008$; OSI.max, $P = 0.01$] and maximum RRT [RRT.max, $P = 0.045$]. ROC analysis revealed AUC values greater than 0.7 for all significant biomarkers. Aneurysm volume [AUC, 0.718; 95% CI, 0.491–0.946] and average OSI obtained from CFD [AUC, 0.774; 95% CI, 0.586–0.961] were retained in the respective logistic regression models.

[1]Department of Radiological and Medical Laboratory Sciences, Nagoya University Graduate School of Medicine, Aichi, Japan
[2]Brain & Mind Research Center, Nagoya University, Aichi, Japan
[3]Department of Radiological Technology, Kariya Toyota General Hospital, Aichi, Japan
[4]Department of Medical Technology, Nagoya University Hospital, Aichi, Japan
[5]Department of Fundamental Development for Advanced Low Invasive Diagnostic Imaging, Nagoya University, Graduate School of Medicine, Aichi, Japan
[6]Department of Radiology, Nagoya University Graduate School of Medicine, Aichi, Japan
[*]Corresponding author: Brain & Mind Research Center, Nagoya University, 1-1-20 Daiko Minami, Higashi-ku, Nagoya, Aichi 461-8673, Japan. Phone: +81-52-719-3154, Fax: +81-52-719-1509, E-mail: isoda@met.nagoya-u.ac.jp

Received: August 7, 2019 | Accepted: November 10, 2019

[7]Department of Diagnostic Radiological Technology, Iwata City Hospital, Shizuoka, Japan
[8]Department of Neurosurgery, Iwata City Hospital, Shizuoka, Japan
[9]Department of Neurosurgery, Komaki City Hospital, Aichi, Japan
[10]Department of Diagnostic Radiology & Nuclear Medicine, Hamamatsu University School of Medicine, Shizuoka, Japan
[11]Hamamatsu Medical Imaging Center, Hamamatsu Medical Photonics Foundation, Shizuoka, Japan
[12]Department of Neurosurgery, Hamamatsu University School of Medicine, Shizuoka, Japan
[13]Department of Neurosurgery, Nagoya University Graduate School of Medicine, Aichi, Japan
[14]Renaissance of Technology Corporation, Shizuoka, Japan
[15]Department of Systems and Control Engineering, School of Engineering, Tokyo Institute of Technology, Tokyo, Japan
[16]Department of Radiology, Stanford University School of Medicine, Stanford, CA, USA
[17]Siemens Healthcare K.K., Tokyo, Japan

Conclusion: Both morphological and hemodynamic biomarkers have significant influence on intracranial aneurysm rupture. Aneurysm size, volume, size ratio, OSI and RRT could be potential biomarkers to assess aneurysm rupture risk.

Keywords: *intracranial aneurysms, rupture risk, hemodynamics, magnetic resonance fluid dynamics (MRFD), 4D Flow MRI, computational fluid dynamics (CFD)*

Introduction

Intracranial aneurysms are pathological dilatations of the arterial walls and an estimated overall prevalence of 3.2% has been reported for a non-comorbid population.[1] The most serious consequence of cerebral aneurysms is their rupture which is the most common cause of non-traumatic subarachnoid hemorrhage (SAH).[2] SAH is associated with high rates of mortality[3] besides resultant cognitive and functional disabilities.[4] An annual rupture rate of 0.95% has been reported for unruptured cerebral aneurysms in a Japanese cohort which excluded patients who underwent treatment[5] whereas an average annual rupture incidence of 1.1% has been reported for a Finnish population in which none of the intracranial aneurysms underwent treatment.[6] Recent advancements in neurovascular imaging and treatment techniques have increased the detection and thereby treatment of intracranial aneurysms. However, treatment of unruptured intracranial aneurysms carries the risk of associated morbidity and mortality rates regardless of their benefits. Hence, deciding which aneurysms should undergo treatment is of vital importance. Despite the claims of natural course of intracranial aneurysms to be depend on aneurysm size, shape, location, patient age, smoking status, hypertension, alcohol consumption, family history and polycystic kidney disease[5–9] the decision making in treatment is mainly based on the aneurysm size and location in the clinical setting. Nevertheless, the fact that small aneurysms also rupture and that some larger aneurysms appear to be stable over time in follow-up studies makes these decisions controversial and necessitate systematic and profound analysis to be carried out with respect to rupture risk assessment.

Hemodynamics is considered as a regulating factor of blood vessel structure and influences formation of vascular pathology such as atherosclerosis, aneurysms and arteriovenous malformations.[10] Many researchers have proposed that hemodynamics in and around intracranial aneurysms is a causative factor in aneurysm pathophysiology, which plays a fundamental role in the mechanisms of growth and rupture as well. Hemodynamics is mainly evaluated using computational fluid dynamics (CFD)[11–12] for intracranial arteries and aneurysms. However, another means of hemodynamic analysis is magnetic resonance fluid dynamics (MRFD)[13–15] which is performed utilizing 3D cine phase-contrast MR imaging (3D cine PC MRI), which is concurrently referred to as 4D Flow MRI.[16] Several recent studies have investigated morphological and hemodynamic parameters to assess the rupture risk of intracranial aneurysms and have found significant results with respect to aspect ratio,[17] size ratio,[18] presence of blebs,[5] nonsphericity index (NSI),[19] inflow concentration index,[20] energy loss,[21] pressure loss coefficient[22] and wall shear stress derivatives.[23–28] However, all of these studies are based on CFD analysis and none of these studies had used patient specific inflow–outflow boundary conditions for the analysis which is a major limitation. In addition, to our knowledge, no rigorous intracranial aneurysm rupture risk assessment study has been reported that utilizes MRFD analysis with representative larger samples rather than case reports. Thus, the aim of our study was to evaluate *in vivo* hemodynamic and morphological biomarkers of intracranial aneurysms, using MRFD and MR-based patient specific CFD in order to assess the risk of rupture.

Materials and Methods

This study was approved by relevant Institutional Review Boards and informed consent had been taken from the patients whose image data were utilized. 48 intracranial aneurysms (10 ruptured aneurysms and 38 unruptured aneurysms) were retrospectively analyzed in the present study, with the intention of identifying morphological and hemodynamic biomarkers for aneurysm rupture using MRFD and CFD utilizing patient specific vessel geometry and patient specific inflow–outflow boundary conditions.

Study subjects

Our data base consisted of 297 intracranial aneurysms of 203 patients who had been followed up after the initial diagnosis. 3D time-of-flight magnetic resonance angiography (3D TOF MRA) and 3D cine PC MRI data of intracranial aneurysms which had been followed up at our three affiliated institutes contributing to our database from 2005 to 2018 were reviewed in the current investigation. Each case had undergone 3D TOF MRA and 3D cine PC MRI at least once during the follow-up. Saccular intracranial aneurysms, consisting both lateral wall and bifurcation type were included in the study. Of 297 aneurysms, seven aneurysms had undergone 3D cine PC MRI before rupture enabling the analysis of pre-rupture status exclusively while four cases had undergone 3D cine PC MRI immediately or few days after rupture. Careful inspection was carried out to confirm vasospasm or any geometric change caused by the rupture for these four cases. As a result, three cases were included in the study and

one case was excluded due to the presence of vasospasm. Thus 10 ruptured aneurysms were selected to "ruptured group". Average time duration from image acquisition to rupture date was 56 months for the aneurysms which ruptured during follow-up and average time duration from aneurysm rupture to imaging date was 3 days for the aneurysms without follow-up before rupture.

The aneurysms those did not rupture during the follow-up were screened for inclusion to the "unruptured group". Inclusion criteria for the "unruptured group" were the aneurysms located in similar sites as the ruptured group with no evidence of SAH and with at least 20 months of follow-up time. This resulted in 182 aneurysms. Subsequent exclusion criteria were the aneurysms which underwent endovascular treatment (109), giant intracranial aneurysms (size >10 mm) or aneurysms of size <3 mm (27), aneurysms with arteriosclerotic changes (2), aneurysms with improper velocity encoding (VENC) settings or narrow FOV (6). Accordingly, 144 aneurysms had to be excluded from the "unruptured group", resulting in 38 aneurysms which met all the inclusion and exclusion criteria. Average follow-up time for these 38 unruptured aneurysms was 86 months. Patient clinical information on gender, ethnicity, history of prior subarachnoid hemorrhage, presence of hypertension, diabetes, polycystic kidney disease, connective tissue disease, family history of intracranial aneurysms or SAH, smoking status and alcohol use were acquired for known risk factors of aneurysm rupture for the 48 cases included in the study.

Imaging methods and parameters

1.5T MR scanner (Signa Infinity Twin speed with Excite, GE Healthcare) with 8-channel neurovascular array coil and two 3T MR scanners (Signa HDx 3T, GE Healthcare and MAGNETOM Verio 3T, Siemens Healthcare) with 8- and 12-channel neurovascular array coils were utilized in image acquisition. Three ruptured and six unruptured aneurysms included in the study had been imaged using 1.5T MR scanner whereas 6 ruptured and 22 unruptured aneurysms had been imaged using 3T MR scanner with 8-channel neurovascular array coil. The other 3T MR scanner with 12-channel neurovascular array coil had been utilized in the image acquisition of one ruptured and 10 unruptured aneurysms in the study. The imaging parameters of 3D TOF MRA and 3D cine PC MRI are shown in Table 1.

Magnetic resonance fluid dynamic (MRFD) analysis

Blood flow analysis software, Flova, (Renaissance of Technology Corporation, Hamamatsu, Japan) was utilized for MRFD analysis. First patient-specific vascular geometries were obtained from 3D TOF MRA data. Region growing method and marching cube method were utilized to segment vessel wall geometry. Next 3D velocity vectors obtained from 3D cine PC MRI were loaded over the extracted vessel geometry using Flova. Phase correction processing was performed while registering velocity vectors and phase encoding directions were adjusted accordingly. Manual corrections of vessel surface position were made when and if there was spatial misregistration between the vessel surface and flow velocity vectors. Once the optimum registration of 3D flow velocity vectors over the vessel geometry was attained (Supplementary Fig. 1; Supplementary materials are available online.) geometric measurements of the aneurysm and its parent artery were carried out. Subsequently, analysis planes for the biomarker calculation were set enabling the calculation of hemodynamic parameters (Supplementary Figs. 2 and 3).

Computational fluid dynamic (CFD) analysis

3D vascular geometries, which were reconstructed using 3D TOF MRA data utilizing Flova, were exported in STL format to create tetrahedral meshes using ICEM CFD version 14.5 (ANSYS, Canonsburg, PA, USA). Maximum edge length was defined as 0.3 mm and minimal was 0.1 mm for each mesh. Surface prism mesh consisted of four prism mesh layers. The thickness of the outermost layer mesh was 0.04 mm and spreading rate was 1.2. The inlet region of vascular geometries were extended in order to obtain fully developed flow. Volume flow rates of vessels were obtained from MRFD analysis to be used as patient specific inlet and outlet boundary conditions. CFD solver software CFX version 14.5 (ANSYS, Canonsburg, PA, USA) was used to compute velocity biomarkers by solving Navier–Stokes equation. Liquid was set as incompressible Newtonian fluid, density was set to 1054 kg/m^3 and dynamic viscosity was set to 3.8 mPa·s. Vascular walls were assumed to be rigid and non-slip. Intervals of cardiac cycles were divided into 100 steps. Two cardiac cycles were simulated and the results of the second cycle were taken for the calculation of hemodynamic biomarkers to ensure numeric stability. Analysis planes placement and hemodynamic biomarker calculation were proceeded using CFD-Post 14.5 (ANSYS, Canonsburg, PA, USA).

Morphological biomarkers

Six morphological biomarkers denoting aneurysm size and shape measures, namely size, volume, aspect ratio, size ratio, presence of blebs and NSI were investigated in this study. Size was defined as the maximum diameter of the aneurysm and both size and aneurysm volume were measured using MRFD analysis. Aspect ratio, a measure of aneurysm ellipticity, which has been initially proposed by Ujiie et al.[17] was defined as the ratio of the maximum perpendicular height to the neck diameter of the aneurysm in the present study. Size ratio, originally proposed by Dhar et al.,[18] was defined as the ratio of the maximum aneurysm height to the parent vessel diameter. Aneurysm blebs were defined as irregular protrusions[5] or lobulations of the aneurysm wall and the presence or absence of blebs were confirmed after careful examination of created 3D vessel geometries, by an experienced neuroradiologist and the main investigator of the study. NSI, which was introduced by Raghavan et al.,[19] is a collective measure

Table 1 MR imaging parameters used in the study

Sequence	1.5T MR scanner with an 8-channel head array coil (Slew rate, 77 T/m/s)		3T MR scanner with an 8-channel neurovascular array coil (Slew rate, 150 T/m/s)		3T MR scanner with a 12-channel head matrix coil (Slew rate, 200 T/m/s)	
	3D TOF MRA	3D cine PC MR	3D TOF MRA	3D cine PC MR	3D TOF MRA	3D cine PC MR
Slice orientation	Transaxial	Transaxial	Transaxial	Transaxial	Transaxial	Transaxial
TR (ms)/TE (ms)/NEX	30/2.6/1	9/3/1	26/3.1/1	5.3/2.4/1	25.0/4.67/1	7.81/3.88/1
Flip angle (°)	15	15	20	15	18	15
FOV (mm)	200 × 200 × 105	160 × 160 × 32	192 × 192 × 102	160 × 160 × 32	160 × 160 × 72	160 × 160 × 30–40
Matrix	320 × 224 × 176 (512 × 512 × 176*)	160 × 160 × 40 (256 × 256 × 40*)	512 × 192 × 204 (512 × 512 × 204*)	160 × 160 × 32 (256 × 256 × 64*)	320 × 320 × 144 (640 × 640 × 144*)	160 × 160 × 30–40 (320 × 320 × 30–40*)
Voxel size (mm^3)	0.63 × 0.89 × 0.6 (0.39 × 0.39 × 0.6*)	1 × 1 × 0.8 (0.63 × 0.63 × 0.8*)	0.38 × 1 × 0.5 (0.38 × 0.38 × 0.5*)	1 × 1 × 1 (0.63 × 0.63 × 0.5*)	0.5 × 0.5 × 0.5 (0.25 × 0.25 × 0.5*)	1 × 1 × 1 (0.5 × 0.5 × 1*)
VENC (cm/s)	N/A	100	N/A	120	N/A	120
Number of phases	N/A	20	N/A	20	N/A	19**
Parallel imaging	N/A	ARC	N/A	ARC	N/A	GRAPPA
Acceleration factor	N/A	2	N/A	2	N/A	2
View per segment	N/A	4	N/A	4	N/A	1–2
ECG gating or triggering	N/A	Retrospective	N/A	Retrospective	N/A	Prospective
Bandwidth (Hz/pixel)	122	488	122	488	220	473
Acquisition time	4 min 48 s	6 min 58 s	5 min 39 s	9 min 36 s	11 min 51 s	26 min 21 s**

*Zero-filled interpolation processing. **Average. ARC, Autocalibrating Reconstruction for Cartesian sampling; ECG, electrocardiogram; FOV, field of view; GRAPPA, GeneRAlized auto calibrating Partially Parallel Acquisitions; MRA, magnetic resonance angiography; N/A, not applicable; NEX, number of excitation; PC, phase-contrast; T, tesla; TE, echo time; TOF, time of flight; TR, repetition time; VENC, velocity encoding.

of undulations and ellipticity of the aneurysm and was calculated using the following equation:

$$\mathrm{NSI} = 1 - (18\pi)^{1/3} \cdot \frac{V^{2/3}}{S}$$

where V and S are volume and surface area of the aneurysm. NSI was investigated in the present study to represent quantification of aneurysm surface irregularity while taking the shape of aneurysm into account.

Hemodynamic biomarkers

Four main hemodynamic parameters were investigated in this study. One parameter, the inflow concentration index (ICI),[20] was chosen as a velocity biomarker. The other three parameters were derivatives of wall sheer stress (WSS), which is defined as the multiplication of fluid viscosity and shearing velocity of neighboring vascular wall.[10] Shearing velocity is calculated by dividing velocity along the wall by distance from wall to the velocity measuring point. WSS related parameters evaluated in this study were time averaged wall shear stress (TAWSS),[23–26] oscillatory shear index (OSI)[27] and relative residence time (RRT).[28] TAWSS, OSI and RRT were further analyzed to obtain spatial average, spatial maximum and spatial minimum values. Supplementary Table 1 provides detailed descriptions of the evaluated hemodynamic biomarkers.

Statistical analysis

IBM SPSS Statistics (version 25) was used for the statistical analysis in order to evaluate the biomarkers between ruptured and unruptured groups. The known risk factors for aneurysm rupture and the presence of blebs between the two groups were compared using Fisher's Exact test. Unpaired Student's *t*-test and Mann–Whitney *U* test were conducted as univariate analysis to detect any significant differences in the biomarkers between these two groups. Shapiro–Wilk test was used to test the normality of data; if the null hypothesis in Shapiro–Wilk test was rejected, Mann–Whitney *U* test was done and these data are reported as medians with interquartile range (IQR); and, if the null hypothesis in Shapiro–Wilk test was not rejected, unpaired Student's *t*-test was done and these data are reported as means with standard deviation (SD). Furthermore, receiver operating characteristic (ROC) analysis was performed for the selected statistically significant biomarkers, and area under the curve (AUC) values and optimal threshold using Yuden index were calculated for them. Logistic regression analysis (using backward stepwise elimination method) was also conducted as multivariate analysis with aneurysm rupture status as the dependent variable for the biomarkers which attained statistical significance in the univariate analysis. Logistic regression was performed separately for the morphological biomarkers, the hemodynamic biomarkers derived from MRFD analysis, and for the hemodynamic biomarkers derived from CFD analysis. Correlations between MRFD and CFD based hemodynamic biomarkers were assessed by Spearman's correlation coefficients. All reported *P*-values were two-sided, and *P*-values below 0.05 were considered to indicate statistical significance for all statistical tests.

Results

Forty-eight intracranial aneurysms categorized as ruptured (10 aneurysms) and unruptured (38 aneurysms) were included in the analysis. Ruptured group consisted of one anterior communicating artery (AComA) aneurysm, one middle cerebral artery (MCA) aneurysm, three internal carotid-posterior communicating artery (ICPComA) aneurysms, one internal carotid-anterior choroidal artery (ICAnt.ChoA) aneurysm, one basilar artery tip (BA Tip) aneurysm, two basilar artery-superior cerebellar artery (BASCA) aneurysms and one vertebral artery-posterior inferior cerebellar artery (VAPICA) aneurysm (Supplementary Table 2). Unruptured group comprised seven AComA aneurysms, 16 MCA aneurysms, seven ICPComA aneurysms, two ICAnt.ChoA aneurysms, five BA Tip aneurysms and one BASCA aneurysm.

With respect to the clinically known risk factors for aneurysm rupture, our study did not reveal any statistical significance for any of the assessed risk factors. All the subjects in this study belonged to one ethnicity and none of them have had prior SAH, connective tissue disease, polycystic kidney disease or family history of aneurysm rupture or SAH. Also, presence of hypertension, diabetes, alcohol intake and tobacco intake were not significant with reference to aneurysm rupture. Although female gender was prominent in the ruptured group, gender did not gain statistical significance as a rupture risk discriminant in the present study (Table 2).

Morphological biomarkers

Results of univariate analysis for five morphological biomarkers (size, volume, aspect ratio, size ratio and NSI) are presented in Table 3, where the biomarkers for which the null hypothesis in Shapiro–Wilk test was not rejected are listed as mean ± SD and the biomarkers for which the null hypothesis in Shapiro–Wilk test was rejected are as median (IQR). The aneurysm size ($P = 0.021$), volume ($P = 0.035$) and size ratio ($P = 0.039$) were found to be significantly different between the ruptured and unruptured aneurysms, whereas aspect ratio and NSI were not statistically significantly different. With respect to the presence of blebs, 15 aneurysms with blebs were found in the unruptured group and five aneurysms presented blebs in the ruptured group. Thus, Fishers exact test could not reveal a statistical significance ($P = 0.721$) for the presence of blebs in discriminating aneurysm rupture (Supplementary Table 3). ROC analysis (Fig. 1) revealed AUC values greater than 0.7 for the three significant morphological biomarkers which are presented in Supplementary Table 4 along with the identified optimal threshold, sensitivity and specificity values.

Hemodynamic biomarkers

The univariate analysis results for the hemodynamic biomarkers are presented in Table 4, where the variables are

Table 2 Comparison of clinically known risk factors between the ruptured and unruptured groups

Clinical characteristics		Unruptured group ($n = 38$)	Ruptured group ($n = 10$)	*P*-value
Gender	Female	24	9	0.140
	Male	14	1	
Ethnicity	All subjects belong to one ethnicity			N/A
Prior SAH	Present	0	0	N/A
Hypertension	No	11	4	0.703
	Present	27	6	
Tobacco intake	No	33	7	0.336
	Yes	5	3	
Diabetes	No	35	9	1.000
	Present	3	1	
Alcohol intake	No	32	9	1.000
	Yes	6	1	
Connective tissue disease	Present	0	0	N/A
Polycystic kidney disease	Present	0	0	N/A
Family history of aneurysm or SAH	Present	0	0	N/A

P-value corresponds to the Fisher's Exact Test statistic and statistical significance is set at $P < 0.05$. N/A, not applicable. SAH, subarachnoid hemorrhage.

Table 3 Morphological biomarkers - univariate analysis

Biomarker	Unruptured group	Ruptured group	*P*-value
An. size (mm)	4.975 (2.09)	7.66 (6.23)	0.021*
An. volume (mm^3)	28.038 (42.01)	175.118 (288.66)	0.035*
Aspect ratio	0.601 (0.29)	0.849 (0.58)	0.121
Size ratio	1.048 ± 0.43	1.408 ± 0.62	0.039*
NSI	0.353 ± 0.06	0.329 ± 0.083	0.282

*Statistically significant at $P < 0.05$. Parametric variables are denoted with mean ± SD and nonparametric variables with median (IQR). An. size, size of the aneurysm; An. volume, volume of the aneurysm; NSI, nonsphericity index.

reported in the same way as in Table 3. The MRFD analysis results of hemodynamic biomarkers indicated that the ruptured aneurysms had significantly higher OSI (OSI.max, $P = 0.037$) and significantly higher RRT (RRT.ave, $P = 0.035$) compared with the unruptured aneurysms. Correspondingly, the CFD analysis results demonstrated statistically significant differences between the two groups with respect to OSI (OSI.ave, $P = 0.008$; OSI.max, $P = 0.01$) and RRT (RRT.max, $P = 0.045$). Figures 2 and 3 graphically illustrate the distribution of OSI

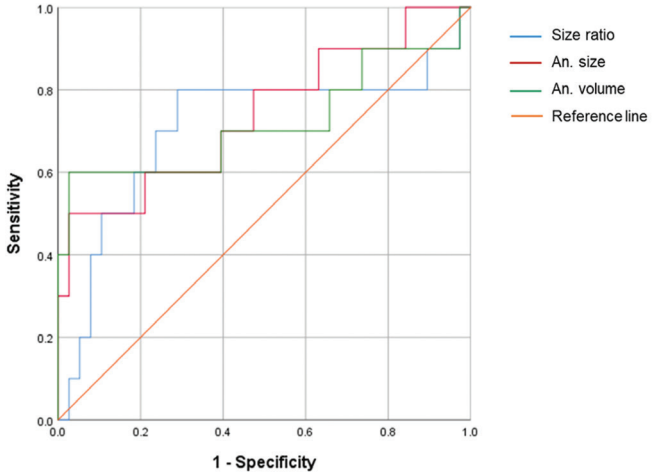

Fig. 1 ROC curves representing significant morphological biomarkers to distinguish aneurysm rupture. ROC curves, receiver operating characteristic analysis curves; An. size, size of the aneurysm; An. volume, volume of the aneurysm.

over the 10 ruptured aneurysms and selected unruptured aneurysms with similar location and shape to match the ruptured aneurysms using MRFD and CFD analyses. However, the other hemodynamic biomarkers (ICI and TAWSS) were not statistically significantly different either in MRFD or in CFD analysis. For the hemodynamic biomarkers which indicated statistically significant differences between the two groups, ROC analysis (Fig. 4) revealed AUC curve values higher than 0.7 and Supplementary Table 4 provides identified threshold values with respective sensitivity and specificity values.

Multivariate analysis

Binary logistic regression analysis was performed to identify independent predictive biomarkers for aneurysm rupture using backward stepwise method. Significant morphological biomarkers and hemodynamic biomarkers were separately regressed in order to determine predictive models. With respect to the morphological biomarkers, the volume of aneurysm (An.Vol) [OR, 1.015; 95% CI, 1.004–1.026] was the only significant predictor of aneurysm rupture which was retained in the model (AUC, 0.718; 95% CI, 0.491–0.946) and its odds of aneurysm rupture (Odd_M) was estimated to be:

$$Odd_M = e^{0.015(An.Vol)-2.652}$$

In the hemodynamic biomarkers derived from the CFD analysis, average OSI (OSI.ave) [OR, $1.942e^{+32}$; 95% CI, $8706.389–4.333e^{+60}$] was the only significant predictor of aneurysm rupture which was retained in the logistic regression model (AUC, 0.774; 95% CI, 0.586–0.961) and its odds of aneurysm rupture (Odd_H) was estimated to be;

$$Odd_H = e^{74.347(OSI.ave)-2.775}$$

However, there were no any significant predictors of aneurysm rupture among the MRFD based hemodynamic biomarkers with respect to multivariate regression analysis.

Table 4 Hemodynamic biomarkers using MRFD and CFD - univariate analysis

Biomarker	MRFD analysis			CFD analysis		
	Unruptured group	Ruptured group	*P*-value	Unruptured group	Ruptured group	*P*-value
ICI	0.436 (0.67)	0.791 (1.04)	0.310	0.842 (0.92)	1.140 (0.80)	0.477
TAWSS.ave	1.353 ± 0.39	1.157 ± 0.41	0.173	2.442 (2.72)	1.852 (2.05)	0.275
TAWSS.max	3.003 ± 1.04	2.868 ± 1.01	0.714	12.412 ± 5.98	13.687 ± 9.15	0.596
TAWSS.min	0.416 ± 0.15	0.331 ± .134	0.103	0.096 (0.24)	0.049 (0.12)	0.104
OSI.ave	0.075 (0.08)	0.120 (0.08)	0.141	0.011 (0.01)	0.026 (0.02)	0.008*
OSI.max	0.442 (0.08)	0.475 (0.05)	0.037*	0.288 (0.15)	0.405 (0.08)	0.010*
OSI.min	0.0019 (0.01)	0.0016 (0.003)	0.264	0.0001 (0.0001)	0.0001 (0.000)	0.879
RRT.ave	1.111 (0.58)	2.012 (1.26)	0.035*	0.879 (1.52)	1.533 (4.54)	0.187
RRT.max	12.377 (19.70)	28.453 (73.24)	0.054	20.277 (62.58)	100.477 (133.72)	0.045*
RRT.min	0.382 (0.20)	0.390 (0.21)	0.630	0.079 (0.07)	0.089 (0.08)	0.526

*Statistically significant at $P < 0.05$. Parametric variables are denoted with mean ± SD and nonparametric variables with median (IQR). MRFD, magnetic resonance fluid dynamics; CFD, computational fluid dynamics; ICI, inflow concentration index; TAWSS, time averaged wall shear stress; TAWSS.ave, spatially averaged TAWSS; TAWSS.max, spatially maximum TAWSS; TAWSS.min, spatially minimum TAWSS; OSI, oscillatory shear index; OSI.ave, spatially averaged OSI; OSI.max, spatially maximum OSI; OSI.min, spatially minimum OSI; RRT, relative residence time; RRT.ave, spatially averaged RRT; RRT.max, spatially maximum RRT; RRT.min, spatially minimum RRT. Unit of TAWSS is Pa.

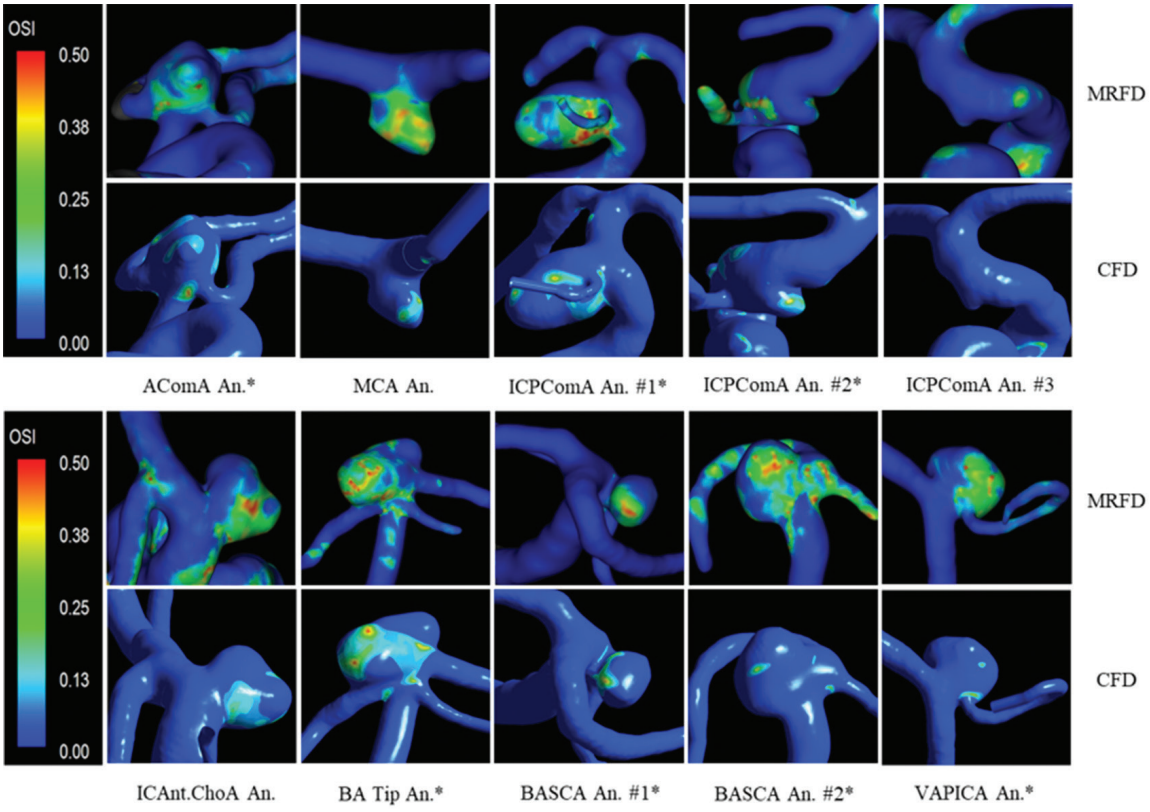

Fig. 2 Distribution of OSI for the 10 ruptured aneurysms using MRFD and CFD analyses. Larger areas of elevated OSI are noticeable in these ruptured aneurysms compared with the representative unruptured aneurysms demonstrated in Fig. 3. MRFD, magnetic resonance fluid dynamics; CFD, computational fluid dynamics; OSI, oscillatory shear index; AComA An., anterior communicating artery aneurysm; ICPComA An., internal carotid-posterior communicating artery aneurysm; ICAnt.ChoA An., internal carotid-anterior choroidal artery aneurysm; MCA An., middle cerebral artery aneurysm; BA Tip An., basilar artery tip aneurysm; BASCA An., basilar artery-superior cerebellar artery aneurysms; VAPICA An., vertebral artery-posterior inferior cerebellar artery aneurysm. *Denotes the aneurysms which underwent 3D cine PC MRI before rupture enabling the assessment of pre-rupture hemodynamics.

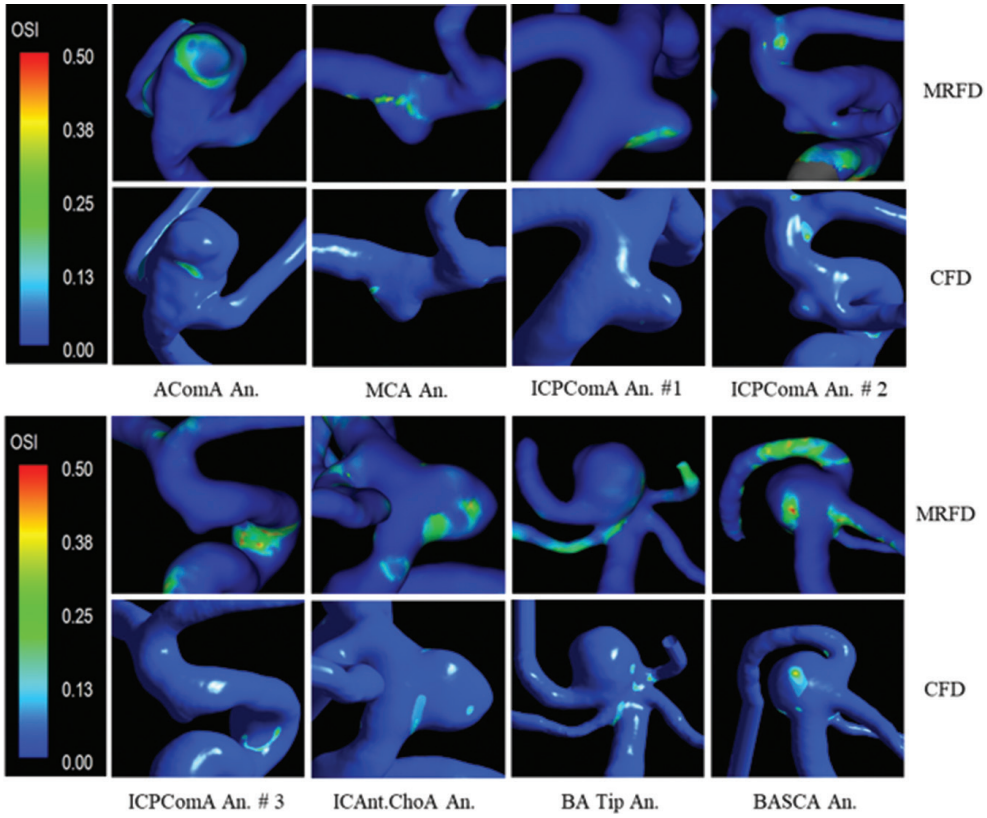

Fig. 3 Distribution of OSI for representative unruptured aneurysms with similar location and geometry as the ruptured aneurysms using MRFD and CFD analyses. Unruptured group included only one BASCA An. and did not include any VAPICA An. due to non-availability. MRFD, magnetic resonance fluid dynamics; CFD, computational fluid dynamics; AComA An., anterior communicating artery aneurysm; ICPComA An., internal carotid-posterior communicating artery aneurysm; ICAnt.ChoA An., internal carotid-anterior choroidal artery aneurysm; MCA An., middle cerebral artery aneurysm; BA Tip An., basilar artery tip aneurysm; BASCA An., basilar artery-superior cerebellar artery aneurysms; VAPICA An., vertebral artery-posterior inferior cerebellar artery aneurysm.

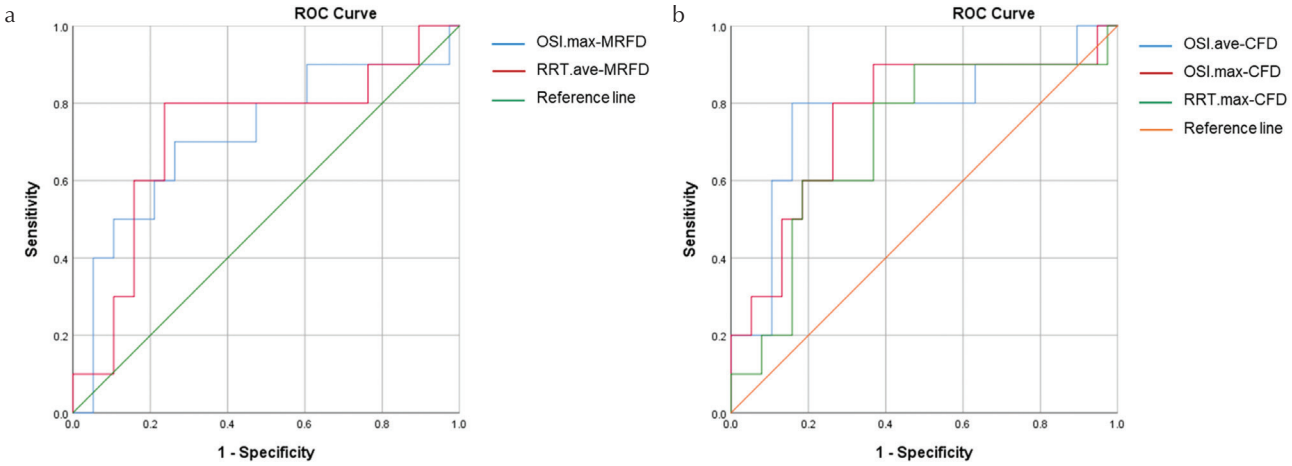

Fig. 4 ROC curves representing significant hemodynamic biomarkers to distinguish aneurysm rupture. Panel (**a**) represents the significant hemodynamic biomarkers obtained from MRFD and (**b**) represents the significant hemodynamic biomarkers obtained from CFD. ROC curves, receiver operating characteristic analysis curves; MRFD, magnetic resonance fluid dynamics; CFD, computational fluid dynamics; OSI, oscillatory shear index; RRT, relative residence time; OSI.max-MRFD, spatially maximum OSI obtained using MRFD; RRT.ave-MRFD, spatially averaged RRT obtained using MRFD; OSI.ave-CFD, spatially averaged OSI obtained using CFD; OSI.max-CFD, spatially maximum OSI obtained using CFD; RRT.max-CFD, spatially maximum RRT obtained using CFD.

Correlations between MRFD and CFD based hemodynamic biomarkers

Spearman's rank correlation coefficients revealed strong positive monotonic correlations between MRFD and CFD for ICI, and moderate positive monotonic correlations for TAWSS.ave, TAWSS.min, OSI.ave, OSI.max, RRT.ave, and RRT.max (Supplementary Table 5). The other biomarkers were unable to reveal such significant correlations. However, all the biomarkers which were found to be significant risk factors for aneurysm rupture showed moderate correlations between

MRFD and CFD. Scatterplots denoting the correlations between MRFD and CFD for the hemodynamic biomarkers are presented in Supplementary Fig. 4.

Discussion

Intracranial aneurysm rupture risk assessment using morphological and hemodynamic biomarkers has been the focus of many recent studies. Despite the fact that treatment decisions are mainly based on aneurysm size and location in the clinical setting, increased attention has been given to hemodynamics in and around aneurysms in research. Our study investigated both morphological and hemodynamic biomarkers with the aim of identifying possible rupture risk discriminants. Although there are many studies which had assessed intracranial aneurysm rupture risk assessment using CFD, no published evidence is found for a comprehensive study that utilized MRFD in this context, to the best of our knowledge. Also, no published evidence can be found for intracranial aneurysm rupture risk assessment study which had utilized patient specific inflow-outflow boundary conditions for CFD analysis together with MRFD analysis besides few studies which had compared inflow hemodynamics of intracranial aneurysms using patient specific CFD and MRFD.[29,30] Hence, we analyzed hemodynamic biomarkers using MRFD analysis in addition to CFD analysis which utilized patient specific vessel geometry as well as patient specific inflow–outflow boundary conditions derived from 3D cine PC MRI. Our study results revealed that the ruptured aneurysms had significantly larger aneurysm size, volume, and size ratio, OSI and RRT compared with the unruptured aneurysms. Specifically, in terms of hemodynamic analysis, MRFD showed statistically significant differences in OSI and RRT comparable with CFD analysis.

Regarding the clinically known risk factors for aneurysm rupture, our study did not show any statistical significance comparable to the study results of the UCAS Japan study.[5] The average size of a ruptured aneurysm in our study was 7.91 mm and the most common location for rupture was ICPComA. UCAS Japan investigators had reported that aneurysms larger than 7 mm and the ones located in the posterior and anterior communicating arteries were more prone to rupture. Despite the fact that our study sample is too small because our ruptured group consisted of only 10 ruptured aneurysms and the unruptured group 38 aneurysms, we could observe similar pattern in epidemiological characteristics in comparison to the UCAS Japan study. However, these epidemiological characteristics could have been affected by the fact that presumably higher risk aneurysms have already undergone treatment resulting an inadequate representation in the rupture risk assessment.

With reference to the morphological biomarkers investigated in the present study, aneurysm size, volume and size ratio showed statistically significant differences between the ruptured and unruptured aneurysms in the univariate analysis, while only aneurysm volume became a significant predictor of aneurysm rupture in multivariate analysis. These results imply that larger aneurysm size and volume can have a significant effect on aneurysm rupture. However, our ruptured group consisted of two aneurysms of size <5 mm and five aneurysms of size <7 mm (Supplementary Table 2). Furthermore, despite our ruptured group included three aneurysms of size greater than 10 mm, giant aneurysms were excluded from the unruptured group to avoid segmentation and hemodynamic analysis restrictions due to the parent artery obstruction caused by the aneurysm. This might have induced some sort of under representation for the medium or small size aneurysms in the ruptured group. Nevertheless, similar findings with respect to size and size ratio of aneurysms as rupture discriminants have been reported by Jing et al.,[23] Chung et al.,[24] Xiang et al.[25] and Amigo and Valencia.[26] The aneurysm volume, which had the most significant effect on rupture risk assessment in our study, have not been studied as an independent morphological biomarker in most of the studies. The aspect ratio, presence of blebs and NSI did not gain statistical significance in our study comparable to Amigo and Valencia[26] but in contrast to several other studies.[17–19,23–25]

In relation to the investigated hemodynamic biomarkers, OSI and RRT were significantly different between the ruptured group and the unruptured group of aneurysms suggesting higher blood oscillations and longer resident times near aneurysm wall can distinguish aneurysm rupture. The longer the time blood spends inside the aneurysm, the slower and circulatory its flow. Hence, these two biomarkers are interrelated. According to the multivariate analysis, OSI was the only significant biomarker for predicting aneurysm rupture risk. It can be speculated that higher blood oscillations for longer time inside the aneurysm is triggering aneurysm wall degeneration and thereby instigate rupture. Meng et al.[31] has proposed that this aneurysm wall degeneration due to high OSI could have been triggered by an inflammatory-cell-mediated destructive remodeling. Similar results have been found by Xiang et al.[25] and Amigo and Valencia,[26] with respect to OSI and RRT as rupture discriminants. Despite the fact that both OSI and RRT are derivatives of WSS, our study was unable to reveal any statistical significance with reference to WSS. However, several studies have reported WSS in the aneurysm as a significant parameter in the rupture risk assessment.[23–26] In addition, ICI was unable to show a significant effect on the aneurysm rupture risk in the present study in contrast to the initial findings reported by Cebral et al.[20] With respect to another two hemodynamic biomarkers, although we attempted the analysis of EL[21] and PLc,[22] confounding results were observed possibly due to the distinctive ways of approximation of static pressure variable by the fluid dynamic analysis software. Those results are not presented in this study as further scrutiny is warranted regarding the biomarker definitions and way of analysis.

With respect to the observed correlations in hemodynamic biomarkers between MRFD and CFD analyses, TAWSS.ave, TAWSS.min, OSI.ave, OSI.max, RRT.ave, and RRT.max

exhibited moderate positive monotonic correlations whereas ICI verified strong correlation (Supplementary Table 5). However, the rest of the three hemodynamic biomarkers could not reveal such correlations. van Ooij et al.[15] has reported that WSS magnitude estimated by PC MRI is lower compared with CFD and the effect to be more pronounced in systole. This could have affected the correlation results of WSS related biomarkers in our study as well. It should be noted that ICI, which mainly depends on flow velocity, had revealed strong correlation between MRFD and CFD. The spatial minimum values of both OSI and RRT could not reveal any correlation possibly due to the fact that CFD simulations are able to output very small numbers compared with MRFD software. Furthermore, it can be reflected that increased spatial resolution in MRFD along with larger sample size would result better correlations between MRFD and CFD.

In the view of hemodynamic analysis methods, although CFD is recognized as the standard criterion, it depends on many assumptions and substantial time is needed for the simulations to be run in addition to the considerable time and effort needed in the pre- and post-analysis methods in obtaining biomarkers. On the other hand, MRFD needs lesser time and personnel effort despite its low resolution compared with CFD in assessing arteries with small caliber.[32] It is reflected that MRFD is more feasible in the clinical setting whereas CFD would be appropriate for the experimental and research setting. In the present study, the statistically significant hemodynamic biomarkers between the ruptured and unruptured groups showed the same pattern in both MRFD and CFD-based results. Hence, in the context of assessing intracranial aneurysm rupture risk, MRFD could be utilized.

In comparison to the available published data on intracranial aneurysm rupture risk assessments, an important merit of the present study is utilizing both MRFD and CFD analyses for the hemodynamic biomarker assessment. Moreover, the use of patient specific inflow–outflow boundary conditions validates our CFD results in contrast to using representative normal subject's velocity profile along with additional assumptions for all the cases. Also, despite the fact that current study is not a case control study like the ones reported by Skodvin et al.[33] and Chung et al.[24] our unruptured group was scrutinized to match the locations with the ruptured group. Yet the unruptured group was unable to represent VAPICA aneurysm, due to non-availability of an unruptured aneurysm in the same location in our data base.

Even though 3D rotational angiography (3DRA) and computed tomography angiography (CTA) have been generally used for vessel geometry in morphological and hemodynamic analyses of intracranial aneurysms due to its high spatial resolution, we utilized 3D TOF MRA for vessel geometry creation. For one reason, the noninvasiveness and comparatively low cost of 3D TOF MRA has made it the most widely used imaging method for intracranial aneurysms during follow-up and on the other hand published evidence not only suggest that CT, MRI and 3DRA adequately reproduce aneurysm geometry and allow meaningful CFD analysis but also revealed that MRI is 2.5 times better than CT with respect to mean reconstruction errors.[34] In addition, Ren et al.[35] has reported that CTA and MRA have no significant differences in reproducing intracranial aneurysm geometry. We did not use magnitude images derived from 3D cine PC MRI as the vessel geometry and rather opted for 3D TOF MRA for two reasons. First, the spatial resolution and signal intensity of vessels of 3D TOF MRA were superior than those of magnitude images derived from 3D cine PC MRI. Second, we used thicker slab 3D TOF MRA data, as CFD analysis necessitates geometric information of upper and lower stream vessels. However, the use of 3D TOF MRA instead of magnitude image of 3D cine PC MRI resulted in occasional misregistration of velocity vectors, which had to be manually corrected.

Although seven out of the ten ruptured aneurysms had undergone 3D cine PC MRI before rupture, the rest of the three aneurysms were imaged immediately or few days after rupture. In spite of our careful scrutiny to exclude any geometric change or vasospasm for these three cases, this could be a limitation of our study. Another limitation of our study could be not discriminating stable and unstable aneurysms in the unruptured group. However, according to a recent study carried out by Chung et al.,[24] which compared the hemodynamics and geometries of stable, unstable, and ruptured aneurysms, collectively analyzing stable and unstable aneurysms together as unruptured aneurysms against ruptured aneurysms permit the characterization of biomarkers due to higher prevalence of stable aneurysms in an unruptured population. One more limitation of our study could be incorporating MR imaging obtained at both 1.5 and 3T field strengths for the hemodynamic analysis. The fact that quality of 3D cine PC MRI performed at 3T field strength is higher than 3D cine PC MRI at 1.5T[36] might have affected the quantitative comparison of hemodynamic biomarkers to some extent.

Conclusion

Both morphological and hemodynamic biomarkers have significant influence on intracranial aneurysm rupture. Aneurysm size, volume, size ratio, OSI and RRT could be potential biomarkers to assess aneurysm rupture risk where aneurysm volume and OSI are the most significant predictors of aneurysm rupture.

Acknowledgments

We thank Tetsuya Wakayama, PhD, of GE Healthcare, Tokyo, Japan for his technical supports and Takasuke Ushio, MD for his support for our research.

Conflicts of Interest

Harumi Sakahara, Haruo Isoda and Yasuo Takehara received Expenditure for Associated Projects of Incentive Special

Budget for the Promotion of National University Reform in Management Expenses Grants.

Haruo Isoda received JSPS KAKENHI (Japan Society for the Promotion of Science, Grants-in-Aid for Scientific Research) (Grant Number 25293264).

Takafumi Kosugi is an employee of Renaissance of Technology Corporation, Hamamatsu, Japan. Yoshiaki Komori is an employee of Siemens Healthcare K.K., Tokyo, Japan.

Yasuo Takehara is an endowed chair of Nagoya University supported by a private company; however, the status is irrelevant to the contents of the paper.

The other authors do not have any conflict of interest to disclose.

Supplementary Information

Supplementary Tables 1–5 and Figs. 1–4 are available online.

Supplementary Table 1
Hemodynamic biomarkers assessed in the study.

Supplementary Table 2
Size of the aneurysms in the ruptured group.

Supplementary Table 3
Morphological biomarkers – categorical variable analysis.

Supplementary Table 4
AUC and optimal thresholds for the significant biomarkers.

Supplementary Table 5
Correlation coefficients between MRFD and CFD-based hemodynamic biomarkers.

Supplementary Fig. 1
Illustration of vessel geometry and blood flow velocity vector distribution in and around a representative aneurysm.

Supplementary Fig. 2
Illustration of geometric measurements in and around an aneurysm for biomarker calculation. H, maximum perpendicular height of the aneurysm; ND, aneurysm neck diameter; PAD, parent artery diameter.

Supplementary Fig. 3
Illustration of geometric measurements of an aneurysm for biomarker calculation: aneurysm volume. Aneurysm volume is denoted by the red highlighted voxels, which represents the vessel volume above the neck plane.

Supplementary Fig. 4
Scatterplots of hemodynamic biomarkers obtained from MRFD and CFD. (**a**–**j**), represents scatterplots denoting the correlations obtained for ICI, TAWSS.ave, TAWSS.max, TAWSS.min, OSI.ave, OSI.max, OSI.min, RRT.ave, RRT.max and RRT.min between MRFD and CFD respectively. MRFD, magnetic resonance fluid dynamics; CFD, computational fluid dynamics; ICI, inflow concentration index; TAWSS, time averaged wall shear stress; TAWSS.ave, spatially averaged TAWSS; TAWSS.max, spatially maximum TAWSS; TAWSS.min, spatially minimum TAWSS; OSI, oscillatory shear index; OSI.ave, spatially averaged OSI; OSI.max, spatially maximum OSI; OSI.min, spatially minimum OSI; RRT, relative residence time; RRT.ave, spatially averaged RRT; RRT.max, spatially maximum RRT; RRT.min, spatially minimum RRT.

References

1. Vlak MH, Algra A, Brandenburg R, Rinkel GJ. Prevalence of unruptured intracranial aneurysms, with emphasis on sex, age, comorbidity, country, and time period: a systematic review and meta-analysis. Lancet Neurol 2011; 10:626–636.
2. van Gijn J, Rinkel GJ. Subarachnoid haemorrhage: diagnosis, causes and management. Brain 2001; 124:249–278.
3. Lantigua H, Ortega-Gutierrez S, Schmidt JM, et al. Subarachnoid hemorrhage: who dies, and why? Crit Care 2015; 19:309.
4. Al-Khindi T, Macdonald RL, Schweizer TA. Cognitive and functional outcome after aneurysmal subarachnoid hemorrhage. Stroke 2010; 41:e519–e536.
5. Morita A, Kirino T, Hashi K, et al. The natural course of unruptured cerebral aneurysms in a Japanese cohort. N Engl J Med 2012; 366:2474–2482.
6. Juvela S, Poussa K, Lehto H, Porras M. Natural history of unruptured intracranial aneurysms: a long-term follow-up study. Stroke 2013; 44:2414–2421.
7. Sonobe M, Yamazaki T, Yonekura M, Kikuchi H. Small unruptured intracranial aneurysm verification study: SUAVe study, Japan. Stroke 2010; 41:1969–1977.
8. Can A, Castro VM, Ozdemir YH, et al. Alcohol consumption and aneurysmal subarachnoid hemorrhage. Transl Stroke Res 2018; 9:13–19.
9. Nurmonen HJ, Huttunen T, Huttunen J, et al. Polycystic kidney disease among 4,436 intracranial aneurysm patients from a defined population. Neurology 2017; 89:1852–1859.
10. Malek AM, Alper SL, Izumo S. Hemodynamic shear stress and its role in atherosclerosis. JAMA 1999; 282:2035–2042.
11. Steinman DA. Image-based computational fluid dynamics modeling in realistic arterial geometries. Ann Biomed Eng 2002; 30:483–497.
12. Cebral JR, Yim PJ, Löhner R, Soto O, Choyke PL. Blood flow modeling in carotid arteries with computational fluid dynamics and MR imaging. Acad Radiol 2002; 9:1286–1299.
13. Isoda H, Ohkura Y, Kosugi T, et al. *In vivo* hemodynamic analysis of intracranial aneurysms obtained by magnetic resonance fluid dynamics (MRFD) based on time-resolved three-dimensional phase-contrast MRI. Neuroradiology 2010; 52:921–928.
14. Futami K, Nambu I, Kitabayashi T, et al. Inflow hemodynamics evaluated by using four-dimensional flow magnetic resonance imaging and the size ratio of unruptured cerebral aneurysms. Neuroradiology 2017; 59:411–418.

15. van Ooij P, Potters WV, Guédon A, et al. Wall shear stress estimated with phase contrast MRI in an *in vitro* and *in vivo* intracranial aneurysm. J Magn Reson Imaging 2013; 38:876–884.
16. Markl M, Chan FP, Alley MT, et al. Time-resolved three-dimensional phase-contrast MRI. J Magn Reson Imaging 2003; 17:499–506.
17. Ujiie H, Tamano Y, Sasaki K, Hori T. Is the aspect ratio a reliable index for predicting the rupture of a saccular aneurysm? Neurosurgery 2001; 48:495–502; discussion 502–503.
18. Dhar S, Tremmel M, Mocco J, et al. Morphology parameters for intracranial aneurysm rupture risk assessment. Neurosurgery 2008; 63:185–197.
19. Raghavan ML, Ma B, Harbaugh RE. Quantified aneurysm shape and rupture risk. J Neurosurg 2005; 102:355–362.
20. Cebral JR, Mut F, Weir J, Putman C. Quantitative characterization of the hemodynamic environment in ruptured and unruptured brain aneurysms. AJNR Am J Neuroradiol 2011; 32:145–151.
21. Qian Y, Takao H, Umezu M, Murayama Y. Risk analysis of unruptured aneurysms using computational fluid dynamics technology: preliminary results. AJNR Am J Neuroradiol 2011; 32:1948–1955.
22. Takao H, Murayama Y, Otsuka S, et al. Hemodynamic differences between unruptured and ruptured intracranial aneurysms during observation. Stroke 2012; 43:1436–1439.
23. Jing L, Fan J, Wang Y, et al. Morphologic and hemodynamic analysis in the patients with multiple intracranial aneurysms: ruptured versus unruptured. PLoS One 2015; 10:e0132494.
24. Chung BJ, Mut F, Putman CM, et al. Identification of hostile hemodynamics and geometries of cerebral aneurysms: a case-control study. AJNR Am J Neuroradiol 2018; 39:1860–1866.
25. Xiang J, Natarajan SK, Tremmel M, et al. Hemodynamic-morphologic discriminants for intracranial aneurysm rupture. Stroke 2011; 42:144–152.
26. Amigo N, Valencia Á. Determining significant morphological and hemodynamic parameters to assess the rupture risk of cerebral aneurysms. J Med Biol Eng 2019; 39:329–335.
27. He X, Ku DN. Pulsatile flow in the human left coronary artery bifurcation: average conditions. J Biomech Eng 1996; 118:74–82.
28. Himburg HA, Grzybowski DM, Hazel AL, LaMack JA, Li XM, Friedman MH. Spatial comparison between wall shear stress measures and porcine arterial endothelial permeability. Am J Physiol Heart Circ Physiol 2004; 286:H1916–H1922.
29. Isoda H, Ohkura Y, Kosugi T, et al. Comparison of hemodynamics of intracranial aneurysms between MR fluid dynamics using 3D cine phase-contrast MRI and MR-based computational fluid dynamics. Neuroradiology 2010; 52: 913–920.
30. van Ooij P, Schneiders JJ, Marquering HA, Majoie CB, van Bavel E, Nederveen AJ. 3D cine phase-contrast MRI at 3T in intracranial aneurysms compared with patient-specific computational fluid dynamics. AJNR Am J Neuroradiol 2013; 34:1785–1791.
31. Meng H, Tutino VM, Xiang J, Siddiqui A. High WSS or low WSS? Complex interactions of hemodynamics with intracranial aneurysm initiation, growth, and rupture: toward a unifying hypothesis. AJNR Am J Neuroradiol 2014; 35:1254–1262.
32. Fukuyama A, Isoda H, Morita K, et al. Influence of spatial resolution in three-dimensional cine phase contrast magnetic resonance imaging on the accuracy of hemodynamic analysis. Magn Reson Med Sci 2017; 16: 311–316.
33. Skodvin TØ, Evju Ø, Helland CA, Isaksen JG. Rupture prediction of intracranial aneurysms: a nationwide matched case-control study of hemodynamics at the time of diagnosis. J Neurosurg 2018; 129:854–860.
34. Goubergrits L, Schaller J, Kertzscher U, Petz Ch, Hege HC, Spuler A. Reproducibility of image-based analysis of cerebral aneurysm geometry and hemodynamics: an in-vitro study of magnetic resonance imaging, computed tomography, and three-dimensional rotational angiography. J Neurol Surg A Cent Eur Neurosurg 2013; 74:294–302.
35. Ren Y, Chen GZ, Liu Z, Cai Y, Lu GM, Li ZY. Reproducibility of image-based computational models of intracranial aneurysm: a comparison between 3D rotational angiography, CT angiography and MR angiography. Biomed Eng Online 2016; 15:50.
36. Bammer R, Hope TA, Aksoy M, Alley MT. Time-resolved 3D quantitative flow MRI of the major intracranial vessels: initial experience and comparative evaluation at 1.5T and 3.0T in combination with parallel imaging. Magn Reson Med 2007; 57:127–140.